


Demonstration of $\mathbb{C}P^2$ skyrmions in three-band superconductors by self-consistent solutions of a Bogoliubov–de Gennes model

Andrea Benfenati , Mats Barkman , and Egor Babaev

Department of Physics, The Royal Institute of Technology, SE-10691 Stockholm, Sweden

 (Received 20 April 2022; revised 5 August 2022; accepted 30 September 2022; published 6 March 2023)

Topological defects, such as magnetic-flux-carrying quantum vortices, determine the magnetic response of superconductors and hence are of fundamental importance. Here, we show that stable $\mathbb{C}P^2$ skyrmions exist in three-band $s + is$ superconductors as fully self-consistent solutions to a microscopic Bogoliubov–de Gennes model. This allows us to calculate microscopically the magnetic signatures of $\mathbb{C}P^2$ skyrmions and their footprint in the local density of states.

DOI: [10.1103/PhysRevB.107.094503](https://doi.org/10.1103/PhysRevB.107.094503)

I. INTRODUCTION

Skyrmions are topological solitons that were originally discussed as an effective description of nucleons [1]. Since that first discussion, many generalizations have been proposed [2]. Currently, the most studied case is magnetic skyrmions, which are a topological defect characterized by the so-called $S^2 \rightarrow S^2$ topological map [3]. However, more complex skyrmionic solutions exist in field theories with more components [2]. In particular, early works considered skyrmions in N -component nonlinear σ models with a high broken symmetry [2,4,5]. More complicated skyrmions, with three or more field components, can be characterized by $\mathbb{C}P^{N-1}$ topological invariants. These are much less studied in condensed-matter systems, where high broken symmetries have been relatively rare. Recently, the interest in these objects started to increase [6–14], revealing interesting properties.

In our work we focus on superconducting systems. Previously, it was shown that $\mathbb{C}P^2$ skyrmions are possible in a phenomenological Ginzburg-Landau model describing a three-band $s + is$ superconductor [6,7]. A three-band $s + is$ superconductor [15–18] can be described by a three-component Ginzburg-Landau theory where $U(1) \times U(1) \times U(1)$ symmetry is explicitly broken to $U(1) \times Z_2$ by intercomponent coupling [16,19]. The Ginzburg-Landau-based studies in [6,7] suggest that $\mathbb{C}P^2$ skyrmions can form in $s + is$ superconductors as metastable states, with a higher energy per flux quanta than ordinary vortices. They could be excited by perturbations and be protected against decay by a potential energy barrier. The experimental discovery of $s + is$ superconductivity in $\text{Ba}_{1-x}\text{K}_x\text{Fe}_2\text{As}_2$ was recently reported [20–22], in agreement with theoretical predictions [15–17]. The evidence is based

on the detection and analysis of spontaneous magnetic fields from muon spin relaxation experiments [21,23], the spontaneous Nernst effect [22], and the existence of two phase transitions indicating two broken symmetries [22,24,25]. This is strong motivation to investigate the existence of $\mathbb{C}P^2$ skyrmions in a fully microscopic model, not limited to temperatures near criticality.

In this paper we report the existence of $\mathbb{C}P^2$ skyrmions in fully self-consistent solutions of a three-band Bogoliubov–de Gennes (BdG) model. The model retains microscopic degrees of freedom. Moreover, the microscopic calculations allow us to determine the skyrmions’ signatures in the local density of states.

II. MODEL

We begin by considering the three-component Hubbard model, defined on a two-dimensional square lattice, described by the microscopic Hamiltonian

$$H = - \sum_{\alpha\sigma} \sum_{\langle ij \rangle} \exp(iqA_{ij}) c_{i\sigma\alpha}^\dagger c_{j\sigma\alpha} - \sum_{i\alpha\beta} V_{\alpha\beta} c_{i\uparrow\alpha}^\dagger c_{i\downarrow\alpha}^\dagger c_{i\downarrow\beta} c_{i\uparrow\beta}. \quad (1)$$

Here, $\langle ij \rangle$ denotes nearest neighbor pairs, and $c_{i\sigma\alpha}$ is the fermionic annihilation operator at position i , with spin σ ($\sigma \in \{\uparrow, \downarrow\}$) and in band α ($\alpha \in \{1, 2, 3\}$). We are using a rescaled unit system, where the planar spatial coordinates are measured in units of the lattice spacing, and all energies are measured in units of the hopping parameter (for details see Appendix A). The quartic interaction term, defined by $V_{\alpha\beta} = V_{\beta\alpha}^*$, allows Cooper pairs to form and tunnel between bands, yielding multiband superconductivity. By performing the mean-field approximation in the Cooper channel (for details see Appendix B), we obtain the mean-field Hamiltonian

$$\mathcal{H} = - \sum_{\sigma\alpha} \sum_{\langle ij \rangle} \exp(iqA_{ij}) c_{i\sigma\alpha}^\dagger c_{j\sigma\alpha} + \sum_{i\alpha} (\Delta_{i\alpha} c_{i\uparrow\alpha}^\dagger c_{i\downarrow\alpha}^\dagger + \text{H.c.}), \quad (2)$$

Published by the American Physical Society under the terms of the Creative Commons Attribution 4.0 International license. Further distribution of this work must maintain attribution to the author(s) and the published article’s title, journal citation, and DOI. Funded by Bibsam.

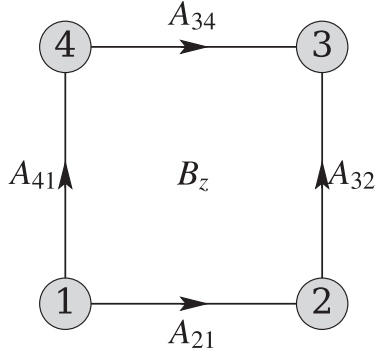


FIG. 1. Illustration of the lattice description of the magnetic field (defined on the plaquette) and the vector potential (defined on the links).

where H.c. denotes Hermitian conjugation. The interaction between the bands is embedded in the self-consistency equations for the gaps, which read

$$\Delta_{i\alpha} = \sum_{\beta} V_{\alpha\beta} \langle c_{\uparrow i\beta} c_{\downarrow i\beta} \rangle. \quad (3)$$

The phase factor $\exp(iqA_{ij})$ accounts for interaction with the magnetic vector potential \mathbf{A} through Peierls substitution [26,27], where

$$A_{ij} = \int_j^i \mathbf{A} \cdot d\ell. \quad (4)$$

The magnetic field is also solved for self-consistently. The current from j to i generated by the fermions equals

$$J_{ij} = - \left\langle \frac{\partial \mathcal{H}}{\partial A_{ij}} \right\rangle = -2q \sum_{\alpha\sigma} \text{Im}[\langle c_{i\sigma\alpha}^\dagger c_{j\sigma\alpha} \rangle \exp(iqA_{ij})]. \quad (5)$$

The current is defined on the links connecting nearest neighboring sites, and we discretize the vector potential in the same way, as shown in Fig. 1. This results in having the magnetic field B_z defined on the lattice plaquettes and equal the discrete curl of the vector potential. Following Fig. 1, we have $B_z = A_{21} + A_{32} - A_{34} - A_{41}$. Following this convention, we can write the magnetic field energy as

$$F_{\text{mag}} = \frac{1}{2} \sum_{\text{plaquettes}} B_z^2, \quad (6)$$

where the sum is carried out over all the plaquettes. The discrete version of Maxwell's equation $\nabla \mathbf{B} - \mathbf{J} = \mathbf{0}$ is

$$\frac{\partial F_{\text{mag}}}{\partial A_{ij}} + \left\langle \frac{\partial \mathcal{H}}{\partial A_{ij}} \right\rangle = 0. \quad (7)$$

The free energy associated with the tight-binding Hamiltonian, up to a constant, equals

$$F_H = \sum_i \Delta_i^\dagger V^{-1} \Delta_i - k_B T \text{Tr} \ln(e^{-\beta \mathcal{H}} + 1), \quad (8)$$

such that the total free energy is $F = F_{\text{mag}} + F_H$.

The self-consistency equations in Eq. (3), along with the Maxwell equation for the magnetic field in Eq. (7), are solved numerically by employing an iterative scheme based on the

Chebyshev spectral expansion method [28–30]. For more details on the iterative scheme, see Appendix C.

A. Gauge and time reversal symmetries

Having introduced coupling between the fermions and the magnetic vector potential using Peierls substitution, the system is now invariant under the gauge transformation

$$c_{i\sigma\alpha} \mapsto \exp(i\chi_i) c_{i\sigma\alpha}, \quad A_{ij} \mapsto A_{ij} + \frac{\chi_i - \chi_j}{q},$$

$$\Delta_{i\alpha} \mapsto \exp(2i\chi_i) \Delta_{i\alpha}. \quad (9)$$

This transformation does not alter the magnetic field or the phase differences between the superconducting gaps. In this notation, the magnetic flux quantum, associated with one vortex, is equal to $\Phi_0 = \pi/q$.

Suppose that (Δ, \mathbf{A}) is a self-consistent solution to our equations. By symmetry, $(\Delta^*, -\mathbf{A})$ is also a solution. The $s + is$ state in the three-band system corresponds to the case where the phase differences between the individual gaps are different from zero and π . This state spontaneously breaks time reversal symmetry since Δ and Δ^* are distinct states (corresponding to $s + is$ and $s - is$ superconducting states, respectively). These two time-reversed states cannot be transformed into each other by a gauge transformation.

B. Skyrmionic index

In this section, we introduce the classification of topological excitations in terms of their topological index. The model contains three complex-valued fields $\Delta = (\Delta_1, \Delta_2, \Delta_3)^T$, defined on a square lattice. We can write $\Delta = \rho \mathbf{Z}$, where $\mathbf{Z} = (Z_1, Z_2, Z_3)^T$ satisfies $|\mathbf{Z}|^2 = 1$ and contains information about the relative phases and magnitudes of the three superconducting gaps. The total density ρ and the relative phases and magnitudes contained in \mathbf{Z} are gauge invariant. If we assume that $\rho > 0$ (that is, the superconducting gaps never vanish simultaneously), the space associated with the relative phases and magnitudes is the complex projective plane $\mathbb{C}P^2$.

For a three-band Ginzburg-Landau model, it was shown that there exists a topological index $Q \in \mathbb{Z}$, associated with the complex projective space $\mathbb{C}P^2$ [7]. Here we will use the corresponding index derived for a lattice in [31], which is defined as a sum over the plaquettes, where each plaquette contains two signed triangles. As in Fig. 1, let 1, 2, 3, and 4 denote the vertices associated with a plaquette in counterclockwise order. One possible choice for the two signed triangles is 123 and 134. The skyrmionic charge density $\rho_{\mathbb{C}P^2}(\text{ABC})$ associated with a signed triangle ABC satisfies

$$\exp[i2\pi \rho_{\mathbb{C}P^2}(\text{ABC})] = \frac{\text{Tr} P_A P_B P_C}{\sqrt{\text{Tr} P_A P_B \text{Tr} P_B P_C \text{Tr} P_C P_A}}, \quad (10)$$

where the matrices P , defined as $P_{\alpha\beta} = Z_\alpha Z_\beta^*$, contain the relative phase and magnitudes of the complex fields at the different vertices [32]. Explicitly, the topological index reads

$$Q = \sum_{\text{plaquettes}} [\rho_{\mathbb{C}P^2}(123) + \rho_{\mathbb{C}P^2}(134)]. \quad (11)$$

III. GROUND STATE AND CRITICAL TEMPERATURE

The ground state is found by considering the case when the superconducting gaps $\mathbf{\Delta} = (\Delta_1, \Delta_2, \Delta_3)^T$ are uniform in the absence of any magnetic field. The self-consistency equations in the multicomponent case are straightforward extensions of the single-component case and read

$$\Delta_\alpha = \sum_\beta V_{\alpha\beta} I(|\Delta_\beta|^2) \Delta_\beta, \quad (12)$$

where

$$I(|\Delta|^2) = \int_{\text{BZ}} \frac{dk_x dk_y}{(2\pi)^2} \frac{\tanh\left\{\frac{1}{2k_B T} E(\mathbf{k}, |\Delta|^2)\right\}}{2E(\mathbf{k}, |\Delta|^2)} \quad (13)$$

and $E(\mathbf{k}, |\Delta|^2) = \sqrt{\xi(\mathbf{k})^2 + |\Delta|^2}$ is the dispersion relation in the presence of the superconducting gap Δ , with $\xi(\mathbf{k}) = -2 \cos k_x - 2 \cos k_y$ being the dispersion relation in the absence of superconductivity. The integral is carried out over the first Brillouin zone $[0, 2\pi) \times [0, 2\pi)$. In order to find the critical temperature at which the superconducting gap vanishes continuously, we can expand Eq. (12) to the lowest order in the gap magnitude, resulting in the linearized gap equation

$$\mathbf{\Delta} = I(0) V \mathbf{\Delta}. \quad (14)$$

It is clear that the critical temperature is determined by the largest eigenvalue V_{\max} of the pairing potential matrix V , such that $1 = I(0) V_{\max}$. The relative phases and magnitudes of the components Δ_α at criticality can be inferred from the corresponding eigenvector.

We now consider the pairing potential matrix $V_{\alpha\beta}$, written in matrix form as

$$V = \begin{pmatrix} v & u & u \\ u & v & u \\ u & u & v \end{pmatrix}, \quad (15)$$

where v is the pairing potential within each band, also called *intra*band pairing, while u is the interaction pairing between different bands, i.e., *inter*band interaction. Diagonalizing the pairing potential matrix V in Eq. (15) gives us two eigenvalues, $V_+ = v + 2u$ and $V_- = v - u$. The eigenvector associated with V_+ is $\mathbf{v}_{+++} = (1, 1, 1)^T / \sqrt{3}$, corresponding to zero phase difference between all three components. The eigenvalue V_- is degenerate, and a possible choice for the two orthonormal associated eigenvectors is

$$\mathbf{v}_{s+is} = \frac{1}{\sqrt{3}} \begin{pmatrix} 1 \\ \omega_3 \\ \omega_3^* \end{pmatrix}, \quad \mathbf{v}_{s-is} = \frac{1}{\sqrt{3}} \begin{pmatrix} 1 \\ \omega_3^* \\ \omega_3 \end{pmatrix}, \quad (16)$$

where $\omega_3 = e^{2\pi i/3}$ is the third root of unity. The eigenvectors $\mathbf{v}_{s\pm is}$ have nonzero phase differences between all three components and are each other's complex conjugates. These three eigenvectors form a complete orthonormal basis, and consequently, the gap vector $\mathbf{\Delta}$ can be expressed as

$$\mathbf{\Delta} = \Delta_{s+is} \mathbf{v}_{s+is} + \Delta_{s-is} \mathbf{v}_{s-is} + \Delta_{+++} \mathbf{v}_{+++}. \quad (17)$$

We are interested in the case when u is negative, such that opposite signs (phase difference π) of the superconducting gaps are favored, and V_- is the largest eigenvalue. In the case of three components, this results in phase frustration since the

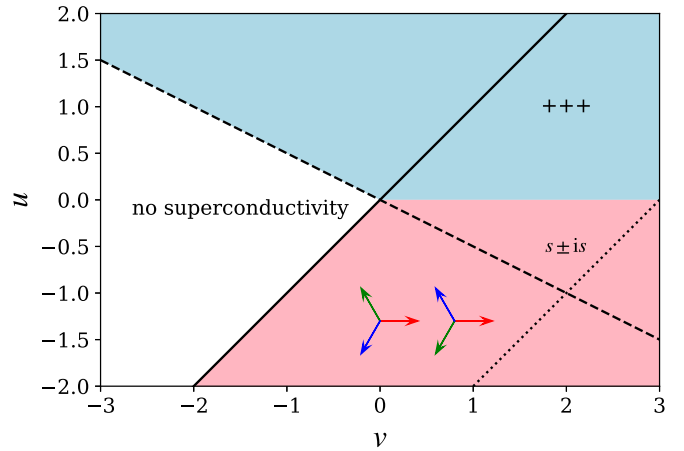


FIG. 2. Phase diagram for the superconducting ground state, where v is the pairing potential within bands and u is the interaction pairing between different bands, as in Eq. (15). When u is positive, the optimal phase difference between the bands is zero, while for negative u , the optimal phase difference is π , resulting in frustration and spontaneous time reversal symmetry breaking (illustrated by the two arrow configurations). This phase diagram holds for all temperatures below the critical temperature. The solid (dashed) line indicates when the pairing potential matrix is singular, i.e., when the eigenvalue V_- (V_+) is zero. No superconductivity is present when both eigenvalues are negative. The dotted line marks where we perform the investigation of skyrmions.

optimal phase difference π cannot be satisfied for all pairs. The resulting ground state $\mathbf{\Delta} \propto \mathbf{v}_{s\pm is}$ spontaneously breaks time reversal symmetry. It is important to note that it is not possible to infer directly from the linearized gap equation the ground state for temperatures below the critical temperature. For example, the state $\mathbf{v}_{++-} = (1, 1, -2)^T / \sqrt{5}$ is also an eigenvector with eigenvalue V_- . Studying the associated free energies shows that the $s \pm is$ state is the ground state for all temperatures below the critical temperature. The phase diagram is shown in Fig. 2.

At the critical lines $V_{\pm} = 0$, the pairing potential matrix is singular, and the free energy in Eq. (8) seems ill defined. However, this is not the case. For example, when $V_+ = 0$, the projection of $\mathbf{\Delta}$ onto the corresponding eigenspace is exactly zero, and the three superconducting gaps $\mathbf{\Delta}$ can always be written as a linear combination of only two order parameters: Δ_{s+is} and Δ_{s-is} . Similarly, when $V_- = 0$, the full three-band system is described by a single order parameter Δ_{+++} . It should be noted that this not only is for the ground state but holds locally for every inhomogeneous gap configuration.

IV. SKYRMION SOLUTIONS

Like the model for conventional superconductors, the three-band model in this paper, described by three complex fields $\mathbf{\Delta} = (\Delta_1, \Delta_2, \Delta_3)^T$, can host topological excitations in the form of vortices. The simplest vortex solution would be the composite vortex, where all three complex fields vanish simultaneously at a joint vortex core. Overlapping vortex cores are favored by the electromagnetic and Josephson couplings [33]. The topological invariant associated with this solution

is the winding number of the complex fields. Fractional vortices, i.e., configurations with winding in only one of the three complex fields, have been found to be stable [9,33] but energetically unfavorable compared to composite vortices in the bulk of the system in a constant external field. The skyrmion solutions, shown previously using Ginzburg-Landau theory for an $s + is$ superconductor [6,7], are situations in which the vortex cores can fractionalize; that is, the vortex cores of the three complex fields do not overlap. The fractionalized vortices populate domain walls. At the domain wall the interaction between fractional vortices is repulsive since phase differences between components have energetically unfavorable values. Hence, the domain wall is stabilized against collapse due to the Josephson interaction together with the magnetic repulsion between the fractional vortices. In these cases, the solution is associated with a topological skyrmionic index \mathcal{Q} , as described in Sec. II B. In this section, we search for such solutions and investigate their properties in a fully microscopic model.

A full phase diagram exploration of these properties is unfeasible. However, by setting $V_- = v - u = 3$ while varying both u and v , we can explore regimes where the interaction between the bands is weak ($|u|$ is small) and where the interaction between the bands is dominant ($|u|$ is large). Since V_- is constant along this line, so is the critical temperature ($k_B T_c \approx 0.46$). This line is marked as a dotted line in Fig. 2. We set $T = T_c/2$ for all simulations, expect for the temperature span considered in Sec. IV B. The numerical solutions we present are obtained from simulating finite-sized systems that are large, such that the skyrmions are sufficiently far away from the boundaries to discard any mesoscopic effects.

A. Skyrmion structure: $\mathcal{Q} = 5$ example

Let us begin by studying the structure of a single skyrmion with skyrmionic topological charge $\mathcal{Q} = 5$, shown in Fig. 3. We set the effective charge $q = 0.15$, the pairing matrix diagonal $v = 2.5$, and off-diagonal $u = -0.5$. The skyrmion is an excitation on top of the $s + is$ ground state, where the phase differences are $\theta_2 - \theta_1 = 2\pi/3$ and $\theta_3 - \theta_1 = -2\pi/3$. The skyrmion consists of five fractional vortices in each superconducting band, that is, with nonoverlapping vortex cores, forming a closed ring. Inside the ring, the phase differences change sign and become an $s - is$ superconducting state. Note also that the vortices form a repeating pattern along the domain wall. The cores are ordered in a 123123... fashion (counterclockwise). The cyclic ordering 132132... is not stable, unless the vortices are replaced with antivortices or if the $s \pm is$ domains are interchanged. A preferential sequence for ordering of fractional vortices, i.e., the skyrmion's chirality, was also found in Ginzburg-Landau models [7].

Our microscopic model allows us to calculate the local density of states (LDOS) at the Fermi energy. It is shown in Fig. 4 together with the magnetic field generated by the skyrmion. The LDOS at energy ϵ is calculated using the quasiparticle wave functions $u_{\uparrow ni}$ and $v_{\downarrow ni}$ with eigenenergy E_n as

$$\text{LDOS}_i(\epsilon) = - \sum_n [|u_{\uparrow ni}|^2 f'(E_n - \epsilon) + |v_{\downarrow ni}|^2 f'(E_n + \epsilon)], \quad (18)$$

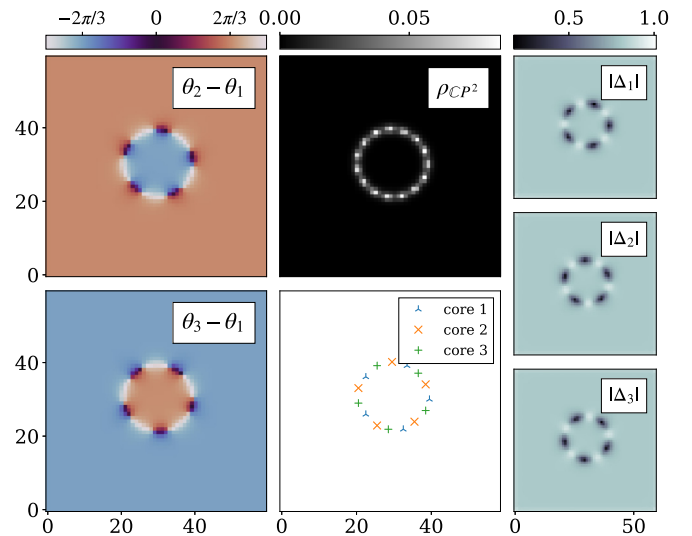


FIG. 3. Example of a skyrmion with $\mathcal{Q} = 5$. The left column shows the two phase differences $\theta_2 - \theta_1$ and $\theta_3 - \theta_1$, showing that the skyrmion forms a circular domain wall, stabilized by the vortices. The second column shows the skyrmion charge density $\rho_C p^2$ and the fractionalization of the vortex cores. The third column shows the absolute value of each superconducting gap. We use intraband pairing $v = 2.5$, interband pairing $u = -0.5$, and effective charge $q = 0.15$.

where $f(x) = (1 + e^{\beta x})^{-1}$ is the Fermi-Dirac distribution and $\beta = 1/(k_B T)$. In this model, the Fermi energy is set at $\epsilon = 0$. Both the magnetic field and the LDOS are localized at the fractional vortex cores. The possibility of resolving the magnetic field peaks of individual vortex cores depends on the skyrmion size in relation to the magnetic field length scale. In the following sections, we investigate how the skyrmion properties depend on the temperature, interband pairing strength, magnetic length scale, and skyrmion index.

B. Skyrmion size dependence on temperature

In this section we investigate how the skyrmion size changes with temperature. We compute the area of the

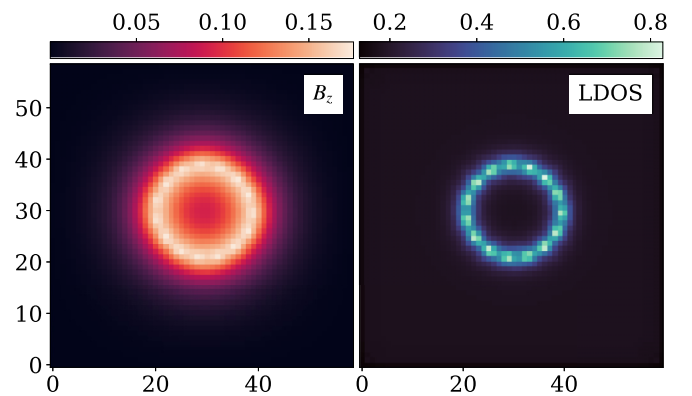


FIG. 4. Magnetic field B_z and local density of states (LDOS) at Fermi energy for the $\mathcal{Q} = 5$ skyrmion in Fig. 3. Both quantities are localized at the domain wall ring and the fractional vortex cores.

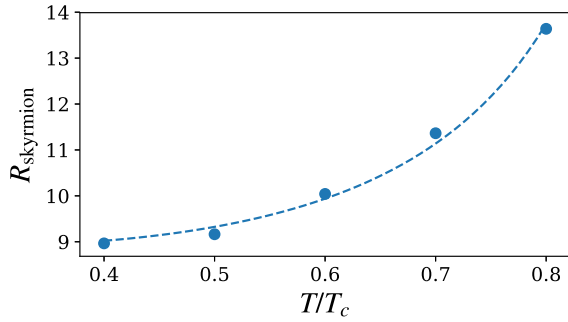


FIG. 5. Skyrmion radius for a $Q = 5$ skyrmion as a function of temperature. Within the considered temperature range, the radius increases with temperature. The dots indicate where simulations were performed and the dashed curve is a fit to the data. We use the same parameters as for the skyrmion in Fig. 3.

skyrmion as

$$A = \frac{1}{2} \sum_i \left[1 - \frac{2}{\sqrt{3}} \sin(\theta_2 - \theta_1)_i \right], \quad (19)$$

and the associated radius $R_{\text{skyrmion}} = \sqrt{A/\pi}$ [34]. The $Q = 5$ skyrmion radius as a function of temperature is shown in Fig. 5 for temperatures $0.4 \leq T/T_c \leq 0.8$. In this temperature range, the skyrmion size increases with temperature.

C. The influence of interband pairing strength

Having demonstrated an example of a stable skyrmion, we now explore its properties as we change the interaction between the bands. To be specific, we study how the skyrmion excitation energy and size change. As previously mentioned, we fix $v - u = 3$ and change both the interband u and the intraband v pairing simultaneously. We parametrize this change as $u = -s$ and $v = 3 - s$ and consider positive values of s . That is, $s = 0$ corresponds to no interaction between the bands, while large s corresponds to interband-dominated pairing. We compute the skyrmion size using Eq. (19). To compute the skyrmion excitation energy $\Delta F_{\text{skyrmion}}$, we calculate the total free energy of the system, from which we subtract the free energy of the ground state. By doing so, we are able to cancel the free-energy contributions coming from the boundary and uniform zones of the gap. The excitation energy and skyrmion radius for a $Q = 5$ skyrmion are shown in Fig. 6. When the interband pairing is weak, the excitation energy is small, and the size of the skyrmion grows. When the interband pairing is strong, the skyrmion shrinks, and the excitation energy increases, both approaching constants in the limit of interband-dominated pairing. The excitation energy is given in units of the excitation energy of a composite vortex. We see that in the limit of weak interband pairing, that is, $s \rightarrow 0$, the skyrmion excitation energy approaches the excitation energy associated with Q vortices. In this limit of weak interband interaction, the skyrmion radius grows, allowing for the peaks of the magnetic field associated with each fractional vortex to be resolved. In the limit of interband-dominated pairing, the skyrmion shrinks such that the field from each fractional vortex no longer can be resolved. In Fig. 6 we show, for comparison, the excitation energy associated with

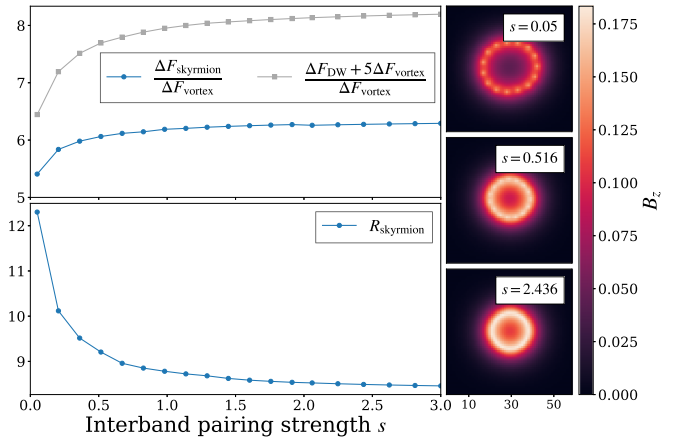


FIG. 6. Excitation energy and skyrmion radius for a $Q = 5$ skyrmion for different strengths of the interband pairing, parametrized by s . Here, $s = 0$ corresponds to no interaction between bands, and $s \rightarrow \infty$ corresponds to interband-dominated pairing. The excitation energy is given in units of the vortex excitation energy. The gray curve shows the energy associated with five vortices separated from a domain wall with length equal to the skyrmion circumference. The fact that the excitation energy of the skyrmion is smaller than the sum of the excitation energy of its constituents shows that domain walls and vortices bind together. The right column shows the magnetic field for some specific values of s . We use effective charge $q = 0.15$, intraband pairing $v = 3 - s$, and interband pairing $u = -s$.

the constituents of the skyrmion: the domain wall and the five composite vortices, considered independently. The excitation energy of the domain wall is calculated as the excitation energy per unit length of a straight domain wall, multiplied by the skyrmion circumference. The fact that the excitation energy of the skyrmion is smaller than the excitation energy of a domain wall and vortices separated shows that skyrmions are formed from an attractive interaction between domain walls and vortices.

D. The influence of the magnetic length scale

In the previous examples, we used a constant value of the effective charge q . In this section, we explore how changing q affects the skyrmion size and energy. For vortices in one-band superconductors, the magnetic field decays on a length scale λ , which depends on the effective charge q . For example, in Ginzburg-Landau theory, λ is proportional to the reciprocal of q . In isotropic multiband models, the tail of the magnetic field of a conventional vortex can be well approximated by $e^{-x/\lambda}$, where λ is the length scale of interest. We consider values of the effective electric charge $q \in [0.144, 0.5]$, for which we compute the excitation energy and magnetic length scale for a single composite vortex, in addition to the excitation energy and radius of a $Q = 5$ skyrmion. The gathered data are presented in Fig. 7, where we show how the excitation energy and size of the skyrmion change as the magnetic length scale is altered. Within the considered parameter regime, both quantities increase linearly with the magnetic length scale λ . In the first approximation, the skyrmion excitation energy can roughly be partitioned

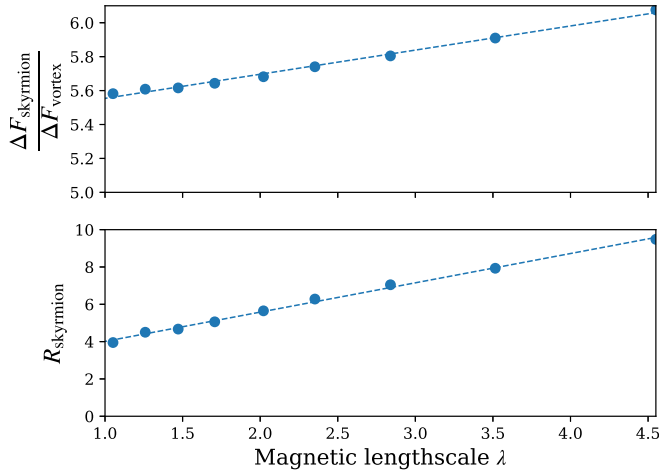


FIG. 7. Excitation energy (in units of vortex excitation energy) and radius for a $Q = 5$ skyrmion for various values of the magnetic length scale λ associated with a composite vortex. In the considered parameters range, both quantities increase linearly with λ . We use intraband pairing $v = 2.5$ and interband pairing $u = -0.5$.

into three parts: the vortex energy, the domain wall energy, and their interaction energy. The domain wall energy scales linearly with the skyrmion radius, which in turn, in the considered regime, scales linearly with λ . We observe that the total excitation energy (i.e. not only the domain wall associated energy) scales linearly with λ . This means that when the magnetic penetration length is relatively large, the excitation energy of flux-carrying skyrmions can be significantly larger than the excitation energy of the corresponding number of flux-carrying vortices. It is unclear whether our range of magnetic length scales is sufficiently wide to extrapolate the trend for even larger values of λ . Numerical limitations on the system size do not allow us to reliably compute skyrmion properties in the BdG model for very large λ (that is, small q), and further investigations are necessary to assess the scaling behavior in this limit.

E. Energy and size scaling with Q

Let us compute the skyrmion excitation energy and the skyrmion radius for different skyrmionic indices Q . The result is shown in Fig. 8, where we consider different magnitudes of the interband pairing controlled by the parameter s , which we introduced previously. We see that both the excitation energy and the radius grow linearly with Q . Increasing the interband pairing strength (increasing s) results in smaller radii and larger excitation energies, as shown already for $Q = 5$ in Fig. 6. Note that for the weakest interaction considered, $s = 0.05$, the stability of the skyrmion is achieved only for topological indices larger than $Q = 2$.

F. Concentric skyrmions

In the previous examples, we considered different skyrmions with different topological indices Q by changing the number of vortices localized at the domain wall. However, it is also possible to change the number of domain walls. In this section, we show that these domain walls can even be concentric. Cocompact skyrmions were previously reported using

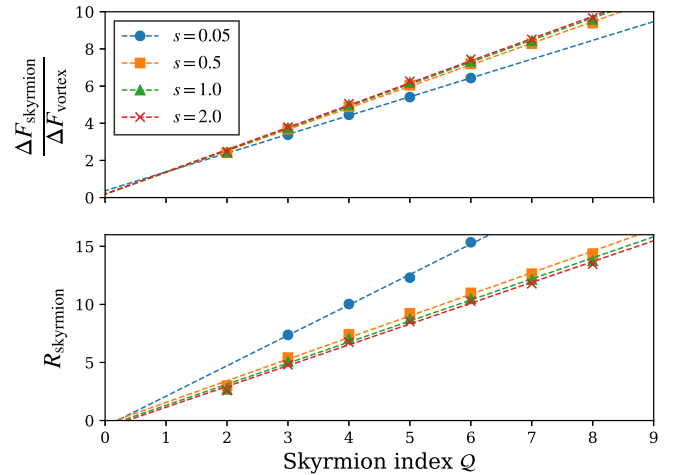


FIG. 8. Skyrmion excitation energy (in units of vortex excitation energy) and skyrmion radius for increasing skyrmionic index Q for different interband pairing strengths s . Both quantities scale linearly with Q . Increasing the interband pairing results in smaller skyrmions with larger excitation energies, as shown in Fig. 6 for $Q = 5$ (we use the same parameters as in Fig. 6).

the Ginzburg-Landau model for $s + is$ superconductors [7]. Similar composite skyrmions have been shown to appear in chiral magnets [35] and liquid crystals [36]. In Fig. 9 we show an example of a concentric skyrmion with $Q = 10$, consisting of two concentric domain walls. Note that on the outer ring, the fractional vortices follow a $123 \dots$ ordering, while on the inner ring, the order is $132 \dots$. The reversal occurs because from the perspective of the outer ring, the regime outside is $s + is$ and the inner one is $s - is$, while for the inner ring, the regimes are the opposite. We can also see that the outer ring forces the inner ring to contract, which is most apparent when studying the magnetic field.

V. CONCLUSION

In conclusion we demonstrated that, at the level of a microscopic Bogoliubov-de Gennes theory in three-band $s + is$ superconductors, there are flux-carrying $\mathbb{C}P^2$ skyrmions. The skyrmions can be viewed as stable bound states of spatially separated fractional vortices and circular domain walls. These solutions were obtained by solving a fully self-consistent three-band Bogoliubov-de Gennes model coupled to a gauge field. In the considered parameter regime, we found that skyrmions are slightly more energetically expensive than vortices per unit of magnetic flux. This suggests that in $\text{Ba}_{1-x}\text{K}_x\text{Fe}_2\text{As}_2$, where the $s + is$ state has been reported, the magnetic response under external field along the c axis should be dominated by ordinary vortices. However, a sufficiently strong quench of a lattice of ordinary vortices may produce $\mathbb{C}P^2$ skyrmions. Recently, more superconducting materials that break time reversal symmetry were discovered [37], for which we can also search for skyrmion solutions. When the superconducting bands are strongly coupled, we find that the magnetic signature of a skyrmion can manifest itself in a scanning superconducting quantum interference device experiment as a washed-out circle, or, more generally, closed stripe,

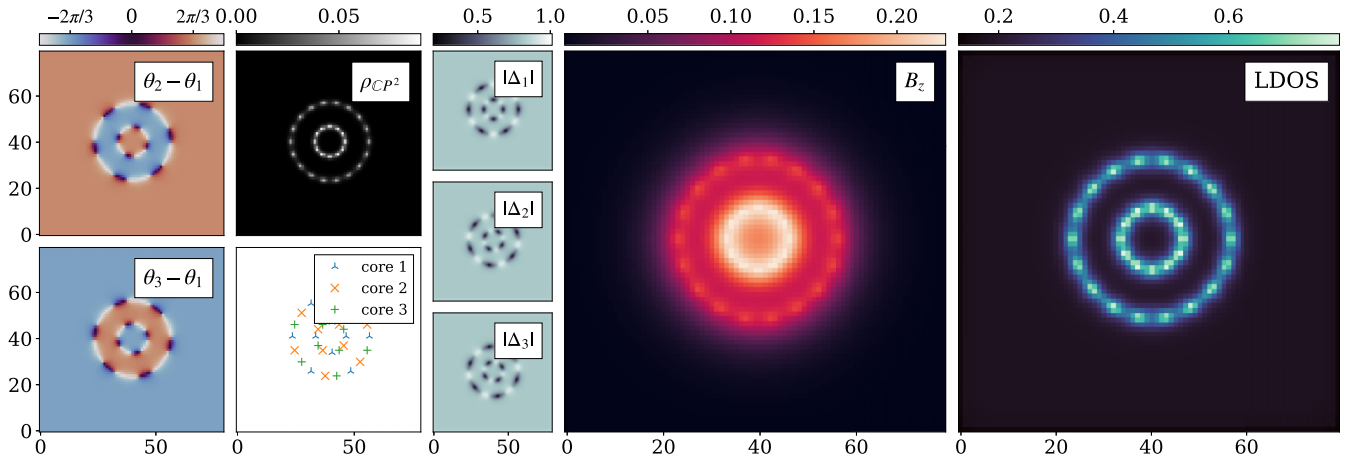


FIG. 9. Example of a concentric skyrmion with $Q = 10$, where the inner ring has four fractional vortices in each band and the outer ring has six. We use the same parameters and show the same quantities as in Figs. 3 and 4.

of magnetic flux. Another possible route to detect skyrmions is scanning tunneling spectroscopy. In fact, the skyrmion solutions that we presented exhibit clear signatures in the local density of states correlated with the position of fractional-flux vortices.

ACKNOWLEDGMENTS

We thank A. Samoilenko for insightful discussions. This work was supported by Swedish Research Council Grants No. 2016-06122 and No. 2018-03659.

APPENDIX A: RESCALING

In dimensionful units, the Hamiltonian for our three-component superconductor, before the mean-field approximation, reads

$$H = -t \sum_{\alpha\sigma} \sum_{\langle ij \rangle} \exp(ieaA_{ij}/\hbar) c_{i\sigma\alpha}^\dagger c_{j\sigma\alpha} - \sum_{i\alpha\beta} V_{\alpha\beta} c_{i\uparrow\alpha}^\dagger c_{i\downarrow\alpha}^\dagger c_{i\downarrow\beta} c_{i\uparrow\beta}, \quad (\text{A1})$$

where t is the nearest-neighbor hopping parameter, e is the electronic charge, and $A_{ij} = \frac{1}{a} \int_j^i \mathbf{A} \cdot d\boldsymbol{\ell}$ accounts for interaction with the magnetic vector potential through Peierls substitution (a is the lattice spacing). The energy associated with the magnetic field equals

$$F_{\text{mag}} = \frac{1}{2\mu_0^{2D}} \sum_{\text{plaquettes}} B_z^2 a^2, \quad (\text{A2})$$

where $B_z = (A_{21} + A_{32} - A_{34} - A_{41})/a$ (following the notation introduced in the main text) and $\mu_0^{2D} = \mu_0/L_z$ is the effective two-dimensional vacuum permeability for the system (L_z is the perpendicular length scale associated with the magnetic field).

Let us introduce a dimensionless system in which we measure all energies in units of the hopping parameter t and the planar coordinates x and y in units of the lattice spacing a ($x = ax'$ and $y = ay'$). Let $H = tH'$ and $F_{\text{mag}} = tF'_{\text{mag}}$, where H'

and F'_{mag} are the rescaled energies. We introduce $V_{\alpha\beta} = tV'_{\alpha\beta}$ for the rescaled Hubbard Hamiltonian. The rescaled magnetic energy equals

$$F'_{\text{mag}} = \frac{1}{2} \sum_{\text{plaquettes}} B_z'^2, \quad (\text{A3})$$

where $\mathbf{B}' = \mathbf{B}a/\sqrt{\mu_0^{2D}t} = \nabla' \times \mathbf{A}'$ and $\mathbf{A}' = \mathbf{A}/\sqrt{\mu_0^{2D}t}$. The Peierls phase reads

$$\frac{e}{\hbar} a A_{ij} = q A'_{ij}, \quad (\text{A4})$$

where $q = \frac{e}{\hbar} a \sqrt{\mu_0^{2D}t}$ and $A'_{ij} = \int_j^i \mathbf{A}' \cdot d\boldsymbol{\ell}'$ are dimensionless. Throughout the main text we use these rescaled coordinates, and for brevity we drop the prime notation.

APPENDIX B: DERIVATION OF THE MEAN-FIELD HAMILTONIAN

The partition function associated with the Hamiltonian in Eq. (1) is

$$Z = \int \mathcal{D}[c^\dagger c] e^{-S(c^\dagger c)}, \quad (\text{B1})$$

where the action S reads

$$S = \int_0^{1/k_B T} d\tau \left[\sum_{ij\sigma\alpha} c_{i\sigma\alpha}^\dagger (\delta_{ij} \partial_\tau + h_{ij\alpha}) c_{j\sigma\alpha} - \sum_{i\alpha\beta} V_{\alpha\beta} c_{i\uparrow\alpha}^\dagger c_{i\downarrow\alpha}^\dagger c_{i\downarrow\beta} c_{i\uparrow\beta} \right], \quad (\text{B2})$$

where $h_{ij} = h_{ji}^*$ is some general quadratic term (such as nearest neighbor hopping). The mean-field approximation is used to rewrite and approximate the quartic interaction term, defined by the interaction strengths $V_{\alpha\beta}$. We assume that the associated interaction matrix V is nonsingular, resulting in three superconducting order parameters (for a discussion of the singular case, see Sec. III). Let $\rho_{i\alpha} = c_{i\downarrow\alpha} c_{i\uparrow\alpha}$, such that the quartic interaction reads $-\sum_{i\alpha\beta} V_{\alpha\beta} \rho_{i\alpha}^\dagger \rho_{i\beta}$. By performing the Hubbard-Stratonovich transformation [38,39] in the

Cooper channel, we have

$$\begin{aligned} & \exp \left\{ \int d\tau \sum_{i\alpha\beta} V_{\alpha\beta} \rho_{i\alpha}^\dagger \rho_{i\beta} \right\} \\ &= \int \mathcal{D}[\Delta^* \Delta] \exp \left\{ - \int d\tau \sum_{i\alpha} \left[\Delta_{i\alpha}^* \rho_{i\alpha} + \Delta_{i\alpha} \rho_{i\alpha}^\dagger \right. \right. \\ & \quad \left. \left. + \sum_{\beta} (V^{-1})_{\alpha\beta} \Delta_{i\alpha}^* \Delta_{i\beta} \right] \right\}, \end{aligned} \quad (\text{B3})$$

where $\Delta_{i\alpha}$ is an auxiliary bosonic field and V^{-1} is the inverse of the coupling matrix. Hence, the partition function becomes

$$\begin{aligned} Z &= \int \mathcal{D}[\Psi^\dagger \Psi] \mathcal{D}[\Delta^* \Delta] \\ & \times \exp \left\{ - \int d\tau \left[\sum_{ij\alpha} \Psi_{i\alpha}^\dagger (\delta_{ij} \partial_\tau + M_{ij\alpha}) \Psi_{j\alpha} \right. \right. \\ & \quad \left. \left. + \sum_{i\alpha\beta} (V^{-1})_{\alpha\beta} \Delta_{i\alpha}^* \Delta_{i\beta} \right] \right\}, \end{aligned} \quad (\text{B4})$$

where we introduced the Nambu spinor notation with

$$\Psi_{i\alpha} = \begin{pmatrix} c_{i\uparrow\alpha} \\ c_{i\downarrow\alpha}^\dagger \end{pmatrix}, \quad \Psi_{i\alpha}^\dagger = (c_{i\uparrow\alpha} \quad c_{i\downarrow\alpha}^\dagger), \quad (\text{B5})$$

and the matrix elements

$$M_{ij\alpha} = \begin{pmatrix} h_{ij} & \delta_{ij} \Delta_{i\alpha} \\ \delta_{ij} \Delta_{i\alpha}^* & -h_{ij}^* \end{pmatrix}. \quad (\text{B6})$$

Let us Fourier transform the Nambu spinors from imaginary time to the Matsubara frequency space, i.e.,

$$\Psi_{i\alpha}(\tau) = \sum_{m=-\infty}^{\infty} \tilde{\Psi}_{i\alpha m} e^{i\omega_m \tau}, \quad (\text{B7})$$

where $\omega_m = 2\pi k_B T (m + 1/2)$ are the Matsubara frequencies for fermions. By integrating out the fermionic degrees of freedom $\tilde{\Psi}_{i\alpha m}$ and $\tilde{\Psi}_{i\alpha m}^\dagger$ we obtain the partition function

$$\begin{aligned} Z &= \int \mathcal{D}[\Delta^* \Delta] \\ & \times \exp \left\{ - \int d\tau \sum_{i\alpha\beta} (V^{-1})_{\alpha\beta} \Delta_{i\alpha}^* \Delta_{i\beta} \right. \\ & \quad \left. + \sum_{\alpha m} \ln \det(\mathbb{1} \omega_m + M_\alpha) \right\}, \end{aligned} \quad (\text{B8})$$

where

$$M_\alpha = \begin{pmatrix} h & \Delta_\alpha \\ \Delta_\alpha^\dagger & -h^* \end{pmatrix} \quad (\text{B9})$$

is a $2N \times 2N$ matrix, with $\Delta_\alpha = \text{diag}(\Delta_{1\alpha}, \dots, \Delta_{N\alpha})$ (N is the total number of sites). By assuming that the auxiliary fields are classical, that is, they have no dependence on τ , we can perform the imaginary time integral, yielding the partition

function

$$Z = \int \mathcal{D}[\Delta^* \Delta] e^{-S'(\Delta^*, \Delta)}, \quad (\text{B10})$$

with

$$S' = \frac{1}{k_B T} \sum_{i\alpha\beta} (V^{-1})_{\alpha\beta} \Delta_{i\alpha}^* \Delta_{i\beta} - \sum_{\alpha m} \ln \det(\mathbb{1} \omega_m + M_\alpha). \quad (\text{B11})$$

At this point, we make the further assumption that the field does not have thermal fluctuation, which means that the only field configuration which does contribute to the partition function is the one which minimizes the action S' . Therefore, we can define the free energy of the model as $F_H = k_B T S'$, obtaining, after summing up the Matsubara frequencies,

$$F_H = \sum_i \Delta_i^\dagger V^{-1} \Delta_i + k_B T \sum_\alpha \text{Tr} \ln f(M_\alpha), \quad (\text{B12})$$

where $f(x) = (e^{\beta x} + 1)^{-1}$ is the Fermi-Dirac distribution and $\Delta_i = (\Delta_{i1}, \Delta_{i2}, \Delta_{i3})^T$. The last step to perform is to find the field configuration which minimizes the free energy, namely,

$$\frac{\partial F_H}{\partial \Delta_{i\alpha}^*} = (V^{-1})_{\alpha\beta} \Delta_{i\beta} + f(M_\alpha)_{i,i+N} = 0. \quad (\text{B13})$$

Following the derivations in [28,29], it is possible to show that the matrix elements of $f(H_\alpha)$ correspond to thermal averages. Explicitly, we have

$$\langle c_{i\uparrow\alpha}^\dagger c_{j\uparrow\alpha} \rangle = f(M_\alpha)_{ji}, \quad (\text{B14})$$

$$\langle c_{i\downarrow\alpha}^\dagger c_{j\downarrow\alpha} \rangle = \delta_{ij} - f(M_\alpha)_{i+N, j+N}, \quad (\text{B15})$$

$$\langle c_{i\uparrow\alpha} c_{j\downarrow\alpha} \rangle = -f(M_\alpha)_{j, i+N}, \quad (\text{B16})$$

yielding the self-consistency equations

$$\Delta_{i\alpha} = \sum_{\beta} V_{\alpha\beta} \langle c_{i\uparrow\beta} c_{i\downarrow\beta} \rangle. \quad (\text{B17})$$

The fields $\Delta_{i\alpha}$ represent the superconducting gaps in each band. We can now insert the equations for the gaps $\Delta_{i\alpha}$ back into the free energy, obtaining, up to a constant,

$$F_H = \sum_i \Delta_i^\dagger V^{-1} \Delta_i - k_B T \text{Tr} \ln(e^{-\beta M} + 1), \quad (\text{B18})$$

where $M = M_1 \oplus M_2 \oplus M_3$. From Eqs. (B17) and (B6) we can see that, following the decoupling in the Cooper channel, the three bands are described by single-band matrices M_α and are coupled through the self-consistency equations.

APPENDIX C: NUMERICAL METHOD DETAILS

In order to solve the mean-field Hamiltonian self-consistently, we need to evaluate thermal averages to compute the superconducting gaps in Eq. (3) and the currents in Eq. (5). The standard approach would be to express these thermal averages in terms of the quasiparticle wave functions $(u_{\uparrow\alpha i}^{(n)}, v_{\downarrow\alpha i}^{(n)})^T$ that satisfy the equation

$$E_{n\alpha} \begin{pmatrix} u_{\uparrow\alpha i}^{(n)} \\ v_{\downarrow\alpha i}^{(n)} \end{pmatrix} = \sum_j \begin{pmatrix} h_{ij} & \Delta_{\alpha i} \delta_{ij} \\ \Delta_{\alpha i}^* \delta_{ij} & -h_{ij}^* \end{pmatrix} \begin{pmatrix} u_{\uparrow\alpha j}^{(n)} \\ v_{\downarrow\alpha j}^{(n)} \end{pmatrix}, \quad (\text{C1})$$

where h_{ij} corresponds to the hopping terms in the Hamiltonian. These quasiparticle wave functions can be found by diagonalizing matrices M_α , which are $2N \times 2N$ Hermitian matrices. However, finding all wave functions and corresponding eigenvalues is computationally expensive. Since we are interested only in local thermal averages, such as those for the superconducting gaps and the currents, it is computationally more efficient to express these thermal averages as matrix elements of $f(M_\alpha)$, where $f(x)$ is the Fermi-Dirac distribution function [see Eqs. (B14), (B15), and (B16)]. Calculating these specific matrix elements is more tractable than full diagonalization of the matrices. We employ the Chebyshev spectral expansion method [28–30], where the Fermi-Dirac distribution is approximated by an expansion in Chebyshev polynomials. For all the simulations, we use 400 polynomials to approximate the distribution function. The number of polynomials needed depends on the smoothness of the Fermi-Dirac distribution, which, in turn, depends on the temperature. For the temperature used in all the simulations we performed, 400 polynomials are sufficient to ensure highly accurate results.

Next, we need to describe the iterative method used to update the magnetic vector potential and the superconducting

gaps. For the superconducting gap we use

$$\Delta_{i\alpha}^{(t+1)} = m\Delta_{i\alpha}^{(t)} + (1 - m) \sum_{\beta} V_{\alpha\beta} \langle c_{\uparrow i\beta} c_{\downarrow i\beta} \rangle^{(t)}, \quad (\text{C2})$$

where $m \in [0, 1)$ is a memory parameter, which is necessary to ensure convergence in certain parameter regimes, where a negative eigenvalue, of the potential matrix V , of large magnitude can destabilize the iterative procedure. The vector potential is updated by performing one gradient descent step

$$A_{ij}^{(t+1)} = A_{ij}^{(t)} - \gamma \left(\frac{\partial F_{\text{mag}}^{(t)}}{\partial A_{ij}} - J_{ij}^{(t)} \right), \quad (\text{C3})$$

where $\gamma = 0.1$ is a constant coefficient. These iterations are continued until a specific convergence criterion is met. We use the requirement that the mean value of the relative change, over all sites (or links for the magnetic vector potential), should be less than 10^{-6} . Efficient calculation of the local density of states can be performed using the Chebyshev expansion method. However, we compute the local density of states using Eq. (18) by performing one diagonalization step after convergence to obtain all information contained in the eigenstates.

-
- [1] T. H. R. Skyrme, A unified field theory of mesons and baryons, *Nucl. Phys.* **31**, 556 (1962).
- [2] N. Manton and P. Sutcliffe, *Topological Solitons*, Cambridge Monographs on Mathematical Physics (Cambridge University Press, Cambridge, 2004).
- [3] N. Nagaosa and Y. Tokura, Topological properties and dynamics of magnetic skyrmions, *Nat. Nanotechnol.* **8**, 899 (2013).
- [4] V. Golo and A. Perelomov, Solution of the duality equations for the two-dimensional $SU(N)$ -invariant chiral model, *Phys. Lett. B* **79**, 112 (1978).
- [5] A. D’Adda, M. Lüscher, and P. Di Vecchia, A 1n expandable series of non-linear σ models with instantons, *Nucl. Phys. B* **146**, 63 (1978).
- [6] J. Garaud, J. Carlström, and E. Babaev, Topological Solitons in Three-Band Superconductors with Broken Time Reversal Symmetry, *Phys. Rev. Lett.* **107**, 197001 (2011).
- [7] J. Garaud, J. Carlström, E. Babaev, and M. Speight, Chiral $\mathbb{C}P^2$ skyrmions in three-band superconductors, *Phys. Rev. B* **87**, 014507 (2013).
- [8] D. L. Kovrizhin, B. Douçot, and R. Moessner, Multicomponent Skyrmion Lattices and Their Excitations, *Phys. Rev. Lett.* **110**, 186802 (2013).
- [9] J. Garaud and E. Babaev, Domain Walls and Their Experimental Signatures in $s + is$ Superconductors, *Phys. Rev. Lett.* **112**, 017003 (2014).
- [10] Y. Lian and M. O. Goerbig, Spin-valley skyrmions in graphene at filling factor $\nu = -1$, *Phys. Rev. B* **95**, 245428 (2017).
- [11] Y. Akagi, Y. Amari, N. Sawado, and Y. Shnir, Isolated skyrmions in the $\mathbb{C}P^2$ nonlinear sigma model with a Dzyaloshinskii-Moriya type interaction, *Phys. Rev. D* **103**, 065008 (2021).
- [12] H. Zhang, Z. Wang, D. Dahlbom, K. Barros, and C. D. Batista, $\mathbb{C}P^2$ skyrmions and skyrmion crystals in realistic quantum magnets, [arXiv:2203.15248](https://arxiv.org/abs/2203.15248).
- [13] Y. Akagi, Y. Amari, S. B. Gudnason, M. Nitta, and Y. Shnir, Fractional skyrmion molecules in a $\mathbb{C}P^{N-1}$ model, *J. High Energy Phys.* **11** (2021) 194.
- [14] Y. Amari, Y. Akagi, S. B. Gudnason, M. Nitta, and Y. Shnir, $\mathbb{C}P^2$ skyrmion crystals in an $SU(3)$ magnet with a generalized Dzyaloshinskii-Moriya interaction, *Phys. Rev. B* **106**, L100406 (2022).
- [15] V. Stanev and Z. Tesanovic, Three-band superconductivity and the order parameter that breaks time-reversal symmetry, *Phys. Rev. B* **81**, 134522 (2010).
- [16] J. Carlström, J. Garaud, and E. Babaev, Length scales, collective modes, and type-1.5 regimes in three-band superconductors, *Phys. Rev. B* **84**, 134518 (2011).
- [17] S. Maiti and A. V. Chubukov, $s + is$ state with broken time-reversal symmetry in Fe-based superconductors, *Phys. Rev. B* **87**, 144511 (2013).
- [18] J. Böker, P. A. Volkov, K. B. Efetov, and I. Eremin, $s + is$ superconductivity with incipient bands: Doping dependence and STM signatures, *Phys. Rev. B* **96**, 014517 (2017).
- [19] J. Garaud, M. Silaev, and E. Babaev, Microscopically derived multi-component Ginzburg–Landau theories for $s + is$ superconducting state, *Phys. C (Amsterdam, Neth.)* **533**, 63 (2017).
- [20] V. Grinenko, P. Materne, R. Sarkar, H. Luetkens, K. Kihou, C. H. Lee, S. Akhmadaliev, D. V. Efremov, S.-L. Drechsler, and H.-H. Klauss, Superconductivity with broken time-reversal symmetry in ion-irradiated $\text{Ba}_{0.27}\text{K}_{0.73}\text{Fe}_2\text{As}_2$ single crystals, *Phys. Rev. B* **95**, 214511 (2017).
- [21] V. Grinenko, R. Sarkar, K. Kihou, C. H. Lee, I. Morozov, S. Aswartham, B. Büchner, P. Chekhonin, W. Skrotzki, K. Nenkov, R. Hühne, K. Nielsch, S.-L. Drechsler, V. L. Vadimov, M. A. Silaev, P. A. Volkov, I. Eremin, H. Luetkens, and H.-H. Klauss, Superconductivity with broken time-reversal symmetry inside a superconducting s -wave state, *Nat. Phys.* **16**, 789 (2020).

- [22] V. Grinenko *et al.*, State with spontaneously broken time-reversal symmetry above the superconducting phase transition, *Nat. Phys.* **17**, 1254 (2021).
- [23] V. L. Vadimov and M. A. Silaev, Polarization of the spontaneous magnetic field and magnetic fluctuations in $s + is$ anisotropic multiband superconductors, *Phys. Rev. B* **98**, 104504 (2018).
- [24] T. A. Bojesen, E. Babaev, and A. Sudbø, Time reversal symmetry breakdown in normal and superconducting states in frustrated three-band systems, *Phys. Rev. B* **88**, 220511(R) (2013).
- [25] T. A. Bojesen, E. Babaev, and A. Sudbø, Phase transitions and anomalous normal state in superconductors with broken time-reversal symmetry, *Phys. Rev. B* **89**, 104509 (2014).
- [26] R. Peierls, Zur theorie des diamagnetismus von leitungselektronen, *Z. Phys.* **80**, 763 (1933).
- [27] R. P. Feynman, R. B. Leighton, and M. Sands, *Mainly Electromagnetism and Matter*, new millennium ed., Feynman Lectures on Physics (Basic Book, NY, USA, 2011), Vol. 2, Chap. 15-5.
- [28] L. Covaci, F. M. Peeters, and M. Berciu, Efficient Numerical Approach to Inhomogeneous Superconductivity: The Chebyshev-Bogoliubov–de Gennes Method, *Phys. Rev. Lett.* **105**, 167006 (2010).
- [29] Y. Nagai, Y. Ota, and M. Machida, Efficient numerical self-consistent mean-field approach for fermionic many-body systems by polynomial expansion on spectral density, *J. Phys. Soc. Jpn.* **81**, 024710 (2012).
- [30] A. Weiße, G. Wellein, A. Alvermann, and H. Fehske, The kernel polynomial method, *Rev. Mod. Phys.* **78**, 275 (2006).
- [31] B. Berg and M. Lüscher, Definition and statistical distributions of a topological number in the lattice $O(3)\sigma$ -model, *Nucl. Phys. B* **190**, 412 (1981).
- [32] Note that here, we are using a different sign convention than in [31], such that $\mathcal{Q} > 0$ for topological excitations associated with positive magnetic flux (for positive charge q and for this order of $s \pm is$ domains).
- [33] E. Babaev, Vortices with Fractional Flux in Two-Gap Superconductors and in Extended Faddeev Model, *Phys. Rev. Lett.* **89**, 067001 (2002).
- [34] Note that the area density in Eq. (19) can exceed 1 and become smaller than 0 by approximately ± 0.077 when the phase difference is close $\pm\pi/2$. However, we have tested that this is not problematic for our purposes. For comparison, using the vortex positions to estimate the size of the skyrmion in Fig. 3 gives an area which is only 1% smaller than the area using the phase difference formula in Eq. (19).
- [35] F. N. Rybakov and N. S. Kiselev, Chiral magnetic skyrmions with arbitrary topological charge, *Phys. Rev. B* **99**, 064437 (2019).
- [36] D. Foster, C. Kind, P. J. Ackerman, J.-S. B. Tai, M. R. Dennis, and I. I. Smalyukh, Two-dimensional skyrmion bags in liquid crystals and ferromagnets, *Nat. Phys.* **15**, 655 (2019).
- [37] S. K. Ghosh, M. Smidman, T. Shang, J. F. Annett, A. D. Hillier, J. Quintanilla, and H. Yuan, Recent progress on superconductors with time-reversal symmetry breaking, *J. Phys.: Condens. Matter* **33**, 033001 (2021).
- [38] J. Hubbard, Calculation of Partition Functions, *Phys. Rev. Lett.* **3**, 77 (1959).
- [39] A. Altland and B. D. Simons, *Condensed Matter Field Theory* (Cambridge University Press, Cambridge, 2010).